Modeling Imbibition in Porous Media with Two-phase flow using a Two-Dimensional Network

K. Shabbir[1], O. Izvekov[1], and A. Konyukhov[1]

[1]Moscow Institute of Physics and Technology

February 28, 2024

Abstract

Simulation of two-phase flow in porous media has many applications in oil recovery, hydrology, electricity production, etc. Classical continuum models consider permeability to be a function of only saturation. Classical continuum models are unable to explain non-equilibrium effects. Advanced continuum models, such as the Kondaurov model considers permeability to be a function of a non-equilibrium parameter in addition to saturation. In order to better understand the non-equilibrium effects, it is necessary to develop non-continuum models at the scale of the pores, for example a network model. The objective of our research is to understand the physical meaning of the Kondaurov non-equilibrium parameter. In this article, we describe the network model we developed for simulating two-phase flow in porous media. At first we determine the pressures in each node by solving a system of linear equations. Then from the known pressures we calculate the flow rates. Lastly we decide an appropriate time step, distribute the fluids in the nodes, and perform displacement of the fluids in the tubes. Our model uses a novel method of distributing different phases in the nodes. We simulated the process of imbibition, where wetting fluid was located in the outer region with thicker radius, and non-wetting fluid in the inner region with thinner radius or finer pores. We measured the saturation of the wetting phase with respect to time in the region of finer pores. Our network model successfully shows that the wetting fluid invades the region of finer pores, and the saturation with respect to time rests to an equilibrium value. Also when produce a variation of radii in the inner region, we clearly observe that the capillary pressure increases with the decrease of wetting fluid in the inner region.

1 Introduction

Simulation of two-phase flow in porous media has applications in oil recovery, hydrology, electricity production where pressurized water is passed through heated pipes and is transformed into steam, etc. Hence it is important to understand and model two-phase flow in porous medium. [21]

1.1 Classical continuum models

Classical continuum models are still commonly used. Darcy's Law is an example of classical continuum model. It is given by:

$$q = -\frac{k}{\mu}\nabla p \tag{1}$$

Here, q is the flow rate, k is the permeability, μ is the coefficient of viscosity, and ∇p is the pressure gradient.

In classical continuum models the permeability is only a function of the saturation of one of the phase.

$$k = k(S) \tag{2}$$

Here, k is the permeability, and S is the saturation of one of the phase.

Saturation S is defined as the ratio between the volume occupied by a phase to the total volume of the void. For wetting phase,

$$S_w = \frac{V_w}{V_{void}} \tag{3}$$

Here, V_w is volume occupied by the wetting phase, V_{void} is total volume of the void. For non-wetting phase,

$$S_{nw} = \frac{V_{nw}}{V_{void}} \tag{4}$$

It is clear that,

$$S_w + S_{nw} = 1 \tag{5}$$

In this article, we denote the saturation of the wetting phase by S.

1.2 Advanced continuum models

The classical continuum models are valid as long as the characteristic time of the processes is much longer than the characteristic time of fluid redistribution in the capillary space.

The fluid distribution can take longer time due to non-equilibrium effects, which occurs when the saturation changes rapidly, or the porous medium is a fractured with blocks and cracks. In these cases, the assumption that $k = k(S)$ is not sufficient and additional parameters are required.

Various advanced continuum models that take such non-equilibrium effects into account. Models of Hassanizadeh [10] [12] and Barenblatt [4] consider that, the permeability k is a function of the rate of saturation change, in addition to the saturation S.

$$k = k(S, \frac{\partial S}{\partial t}) \tag{6}$$

Here,

$$S = S(t) \tag{7}$$

2

The Kondaurov model [19] considers a special non-equilibrium parameter ξ along with saturation S, which relaxes to an equilibrium value. [18]

$$k = k(S, \xi) \tag{8}$$

This parameter ξ is related to S by the differential equation:

$$\frac{\partial \xi}{\partial t} = \Omega(S, \xi) \tag{9}$$

The final objective of our research is to develop a network model which helps us better understand the Kondaurov non-equilibrium parameter ξ.

1.3 Non-continuum models

In order to better understand the non-equilibrium characteristics, it is often necessary to simulate the flow at the scale of pores. Some of the methods of modeling at the scale of pores are, Lattice Boltzmann Method, a direct Navier-Stokes simulation, or a network model. Direct Navier-Stokes simulation provides very accurate results on velocity and pressure distributions, but it is very complicated. Network models are much simpler.

One of the earliest models simulated the flow using a network of electrical resistors [8]. Some of the modern models, such as by Aker et al [2] used an hour glass shaped model of tubes to perform simulation, where the average flow rate was given by the Washburn equation for capillary flow [30]. The disadvantage is that the flow rate must be approximated for cylindrical tube while in their model, the capillary pressure varied depending on its position in the tube.

Our network model uses a novel method of distributing different phases at the nodes. It used only cylindrical tubes, and the flow rate is given by simple equations. In this article we demonstrate the applicability of our model by simulating imbibition.

2 Characteristics of the model

2.1 Approximation of a porous medium

(a) Pore as node, and capillary as tube
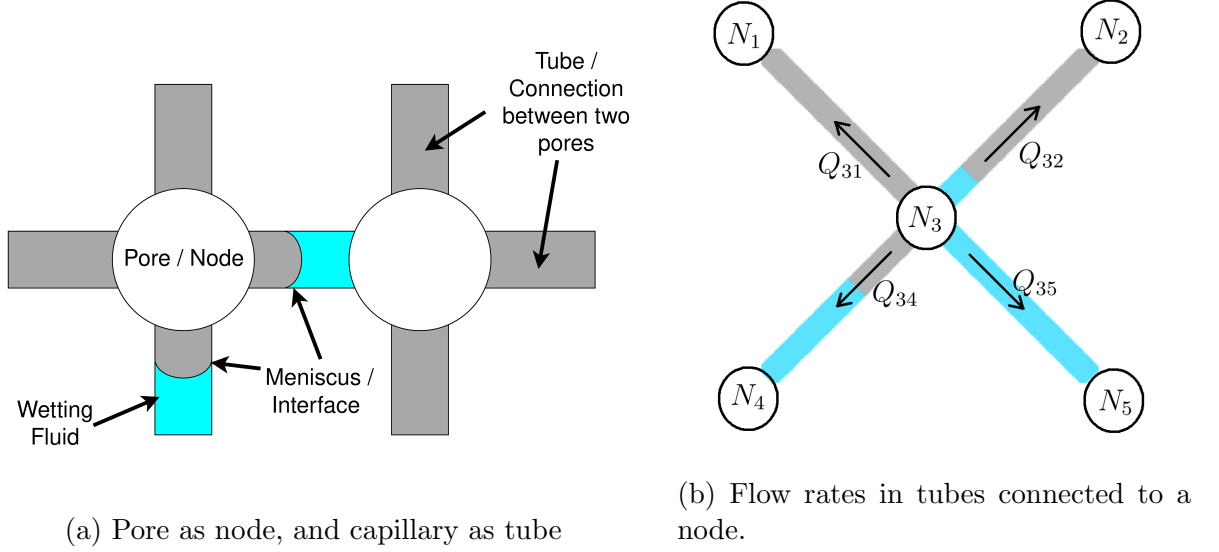
(b) Flow rates in tubes connected to a node.

Figure 1: Network model of porous medium.

A porous medium consists of pores, which are connected by capillaries. The pores are represented by nodes, while the capillaries are represented by tubes, as shown in figure 1a. Our model is two-dimensional. Each node is connected to 4 other nodes through tubes, shown in figure 1b. They may be connected to less than 4 nodes, when they are located on the boundaries. The color cyan denotes wetting fluid, while the color gray denotes non-wetting fluid.

Gravity is ignored. The fluids are not compressible. The volume of the node is not taken into consideration and is assumed to be zero. All tubes are of equal length and cylindrical. The tubes can have different radii. The capillary pressure is zero inside the node. A tube can have a maximum of 2 menisci. The novelty of our model is that during flow, when both cyan and gray fluid enters one node, then the fluids are distributed such that the cyan fluid is distributed first to the thinner tubes. If a tube has more than two meniscus, then there are combined together such that the center of mass of each fluid remains the same.

Note that the assumption of zero volume of node would not change the mixing of different fluids. Let us assume that a node with non-zero volume is filled with gray fluid is invaded by cyan fluid. Since the cyan fluid is distributed first, it immediately reaches the ends of the other tubes connected to the node. The assumption of zero volume of node only affects how the saturation is calculated, never the less it was assumed to be zero to keep the calculations simple.

2.2 Set of linear equations for a node

Let the flow rate in a tube be given by:

$$Q_{ij} = A_{ij}\Delta P_{ij} + B_{ij} \tag{10}$$

4

Here, Q_{ij} is the flow rate form node N_i to node N_j. A_{ij} and B_{ij} are real constants. Here $\Delta P_{ij} = P_i - P_j$, where N_i is kept at a pressure of P_i and N_j at a pressure of P_j. The detailed form is given by equation 38

During simulation, we produce a set of linear equations. We iterate through each node, write equations of flow rates for each tube connected to the node, and equate the sum to zero. For each node, we get one row of the linear equation augmented. For figure 1b:

$$Q_{3j} = A_{3j}\Delta P_{3j} + B_{3j} \tag{11}$$

Due to the conservation of volume, we have:

$$\sum_k Q_{3k} = 0 \tag{12}$$

Where $k = 1, 2, 4, 5$.

Note that all Q's point outward. The Q's will have different signs in order to preserve the law of conservation of volume. For fluid flowing out of N_3, we will have $Q_{3j} > 0$, while for fluid flowing into N_3, we will have $Q_{3j} < 0$.

Let us assume that the pressures at all nodes are known, except N_3. Then, the set of linear equations would look like:

$$\begin{pmatrix} 1 & 0 & 0 & 0 & 0 & P_1 \\ 0 & 1 & 0 & 0 & 0 & P_2 \\ -A_{31} & -A_{32} & (A_{31} + ... + A_{35}) & -A_{34} & -A_{35} & -(B_{31} + ... + B_{35}) \\ 0 & 0 & 0 & 1 & 0 & P_4 \\ 0 & 0 & 0 & 0 & 1 & P_5 \end{pmatrix} \tag{13}$$

2.3 Average Capillary Pressure

The average capillary pressure in a region is defined as:

$$P_c = \frac{\sum \frac{2\sigma}{r_i} s_i \pi r_i^2}{\sum s_i \pi r_i^2} \tag{14}$$

Here σ is the coefficient of surface tension. And r_i is the radius of the tube.

$$s_i = \begin{cases} 0, & \text{even number of meniscus in the tube} \\ 1, & \text{odd number of meniscus in the tube} \end{cases} \tag{15}$$

2.4 Multi-phase flow in a node

The novelty of our model is how we distribute phases in the nodes. When more than one phase flows into a node, the wetting fluid first enters the tube with the thinner radius. This is to minimize the energy of the system. Below is an example:
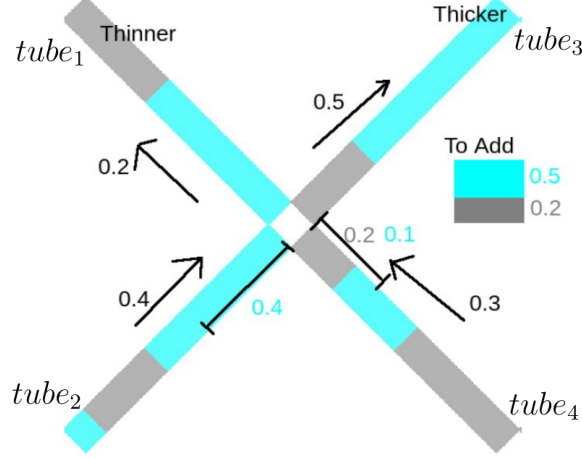
5

Figure 2: Distribution prediction of different fluids in a node.

In figure 2, fluid flows from $tube_2$ and $tube_4$ into $tube_1$ and $tube_3$.

From the calculation of flow rates, we determined that $0.7u.$ (unit volumes) of fluid enters the node, while $0.7u.$ exits the node. They must be equal due to Kirchhoff's law at the node. The total inflow of $0.7u.$ consists of $0.4u.$ from $tube_2$ and $0.3u.$ from $tube_4$. The outflow consists of $0.2u.$ into $tube_1$, and $0.5u.$ into $tube_3$.

Step-1, we calculate the sum of volume of each type of fluid flowing into the node. Here, $tube_2$ provides $0.4u.$ of cyan fluid, while $tube_4$ provides $0.1u.$ of cyan fluid and $0.2u.$ of gray fluid. Summing we obtain $0.5u.$ of cyan fluid and $0.2u.$ of gray fluid, which needs to be distributed to the outflow tubes.

(a) Adding wetting phase to the thinner tube first.
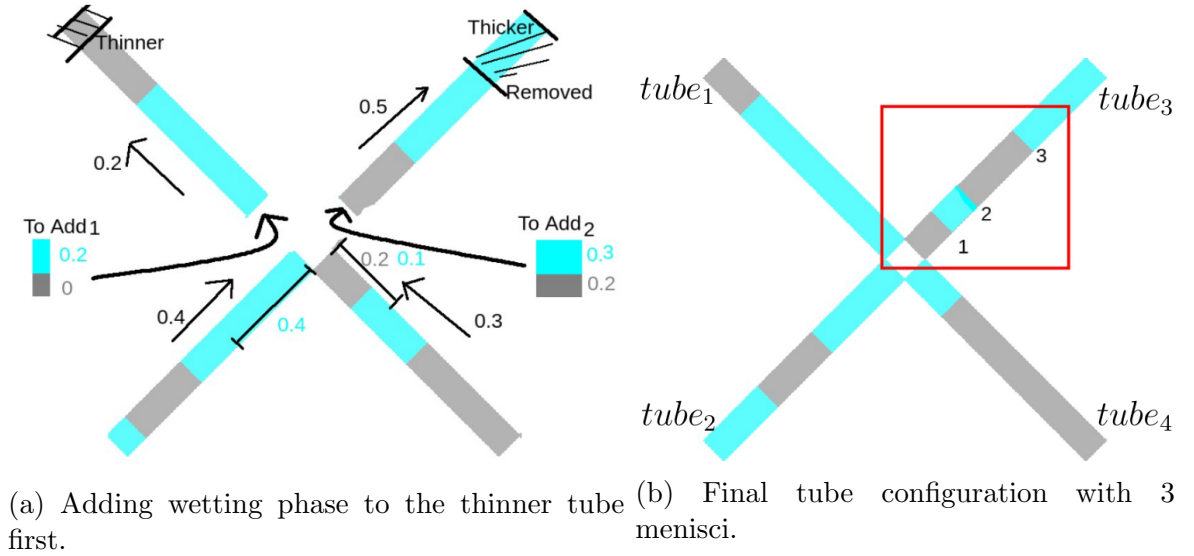
(b) Final tube configuration with 3 menisci.

Figure 3: Occurrence of more than 2 menisci.

Step-2, we allocate this $0.5u.$ of cyan fluid first into the thinner tube. The thinner $tube_1$ takes in $0.2u..$ This allocation space is entirely filled by $0.2u.$ of cyan fluid. Then for the thicker tube, we need to insert $0.5u.$ of fluid into it. $0.3u.$ of cyan fluid is inserted first then $0.2u.$ of gray fluid.

6

In figure 3b, $tube_1$ retains the only meniscus because the end connected to the node initially contained cyan fluid, and we introduced $0.2u.$ of more cyan fluid. The single meniscus was just displaced upwards.

However, in $tube_3$, gray fluid was on the end of the tube connected to the node. We added $0.3u.$ of cyan and $0.2u.$ of gray fluid. Since the cyan fluid entered the thicker tube first, we end up with 3 menisci.

2.5   Recombination

Our data structure was constrained to only allow the case for a maximum of two menisci in a tube. However, we see that in figure 3b that there is possibility of more than 2 menisci occurring after distribution. We show the cases of distributing fluid in the nodes, which results in more than 2 menisci.
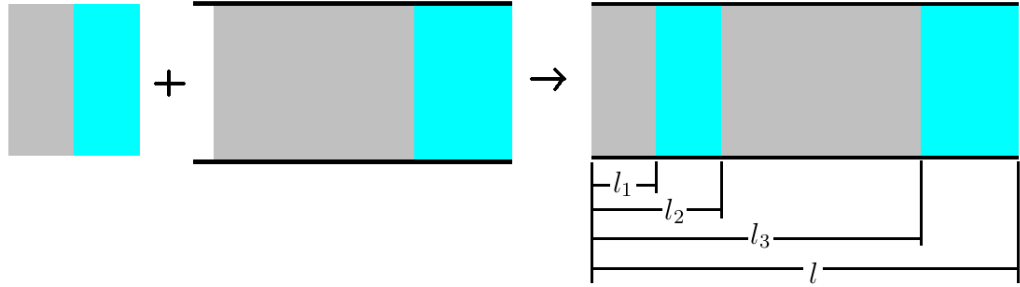

Figure 4: Recombination of 3 menisci

In figure 4 we have a known amount of cyan and gray fluid which we need to insert into the tube. The tube which already consists of both the fluids. The flow is from left to right, so we insert the incoming fluids on the left end of the tube. Note that a block of cyan fluid always ends up in the center as it enters the tube first.

Let l_i denote the location of a meniscus. Since the tube is cylinder, the mass is simply proportional to the length they occupy in the tube, they are given by:

$$m_1 = l_2 - l_1 \tag{16}$$

$$m_2 = l - l_3 \tag{17}$$

Their respective center of masses d_1 and d_2 are given by:

$$d_1 = \frac{l_1 + l_2}{2} \tag{18}$$

$$d_2 = \frac{(l_3 + l)}{2} \tag{19}$$

The center of mass of the cyan fluid in the tube is then given by:

$$d = \frac{m_1 d_1 + m_2 d_2}{m} \tag{20}$$

7

Here,

$$m = m_1 + m_2 \tag{21}$$

We do not change the proportion of fluids in a tube during recombination. Therefore, it can be shown that if we recombine the fluids in a tube such that the center of mass of one of the fluid remained the same, then the center of mass of the other fluid will also remain the same.
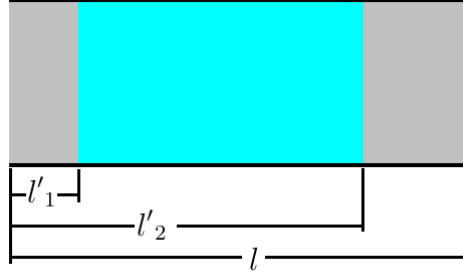

Figure 5: After recombination, we always have 2 menisci

Let l'_i denote the position of meniscus after recombination.

$$l'_1 = d - \frac{m}{2} \tag{22}$$
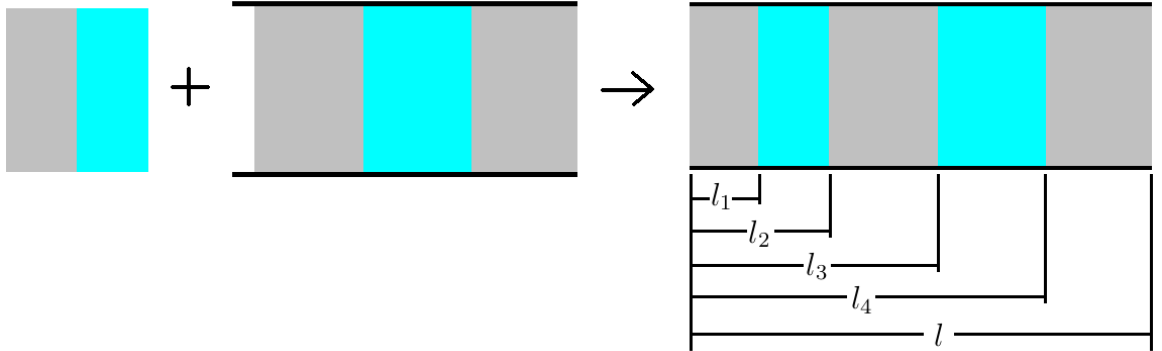
$$l'_2 = d + \frac{m}{2} \tag{23}$$

Figure 6: Recombination of 4 menisci

When there are 4 menisci, we repeat the same process, except here:

$$m_2 = l_4 - l_3 \tag{24}$$

And

$$d_2 = \frac{(l_3 + l_4)}{2} \tag{25}$$

2.6 Flow rate in a tube with one meniscus

At first we derive the equation for flow rate when there is one meniscus present in a tube, then we generalize the case for n menisci. The flow rate of a viscous fluid through a thin tube is given by the Hagen–Poiseuille equation:

$$Q = \frac{\pi}{8\mu}\frac{\Delta P}{l}R^4 \tag{26}$$

Here, Q is the volumetric flow rate in $[m^3/s]$, ΔP is the pressure difference between the ends of the tube, μ is the viscosity in $[kg/m.s]$, l is the length of the tube, R is the radius of the tube.
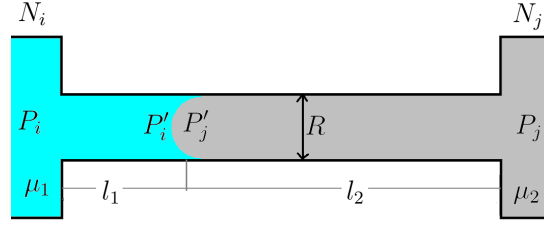

Figure 7: Orientation of the meniscus, the convex side contains wetting fluid while the concave side contains non-wetting fluid.

In figure 7, node N_i kept at a pressure of P_i, and is filled with a wetting fluid of viscosity μ_1. Node N_j kept at a pressure of P_j is filled with a non-wetting fluid of viscosity μ_2. It is evident that the pressure on the convex size or on the part of the wetting fluid is lower.

$$P_i' < P_j' \tag{27}$$

The pressure jump is given by:

$$P_j' - P_i' = \frac{2\sigma}{R} \tag{28}$$

Here, σ is the coefficient of surface tension in $[Pa.m]$ or $[kg/s]$.

Separating figure 7 into two tubes of lengths l_1 and l_2, containing fluids of viscosity μ_1 and μ_2. The flow rates of the tubes, from equation 26 are given by:

$$Q = \frac{\pi}{8\mu_1}\frac{P_i - P_i'}{l_1}R^4 \tag{29}$$

$$Q = \frac{\pi}{8\mu_2}\frac{P_j' - P_j}{l_2}R^4 \tag{30}$$

Due to the law of conservation of volume, the flow rates are equal. Adding the equations 29 and :

$$Q(\mu_1 l_1 + \mu_2 l_2) = \frac{\pi}{8}R^4(P_i - P_j + P_j' - P_i') \tag{31}$$

Substituting the equation 28 about capillary pressure,

$$Q = \frac{\pi R^4}{8Ml}\left(\Delta P_{ij} + \frac{2\sigma}{R}\right) \tag{32}$$

Here,

$$\Delta P_{ij} = P_i - P_j \tag{33}$$

And M is the viscosity parameter:

$$M = \sum_k \mu_k \frac{l_k}{l} \tag{34}$$

Note that the viscosity parameter, remains the same for any number of menisci present in a tube.

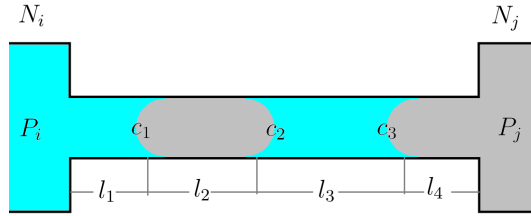## 2.7   Flow rate in a tube with multiple menisci

Figure 8: Capillary pressure contribution, $s = 1$

Let the capillary pressures be denoted by the following:

$$c_1 = -c_2 = c_3 = \frac{2\sigma}{R} \tag{35}$$

Then for figure 8, the flow rate is given by:

$$Q = \frac{\pi R^4}{8Ml}\left(\Delta P_{ij} + c_1 + c_2 + c_3\right) \tag{36}$$

$$Q = \frac{\pi R^4}{8Ml}\left(\Delta P_{ij} + \sum_k c_k\right) \tag{37}$$

Flow rate for an arbitrary number of meniscus for a cylindrical tube, is given by:

$$\boxed{Q = \frac{\pi R^4}{8Ml}\left(\Delta P_{ij} + \frac{2s\sigma}{R}\right)} \tag{38}$$

Where,

$$s(d, n_{mns}) = \begin{cases} -1, & n_{mns} = 1,\ d \text{ points away from } N_i \\ 0, & n_{mns} = 0,\ 2 \\ +1, & n_{mns} = 1,\ d \text{ points towards } N_i \end{cases} \tag{39}$$

Here,

- d, the direction the convex side of the meniscus points towards

- n_{mns}, the number of meniscus in a tube

In our model, the data structure does not accommodate more than 2 meniscus in a tube, hence in the definition of s, $n_{mns} \leq 2$. Shown that, for figure 8, 9a, and 9b, s is 1, -1, and 0 respectively.
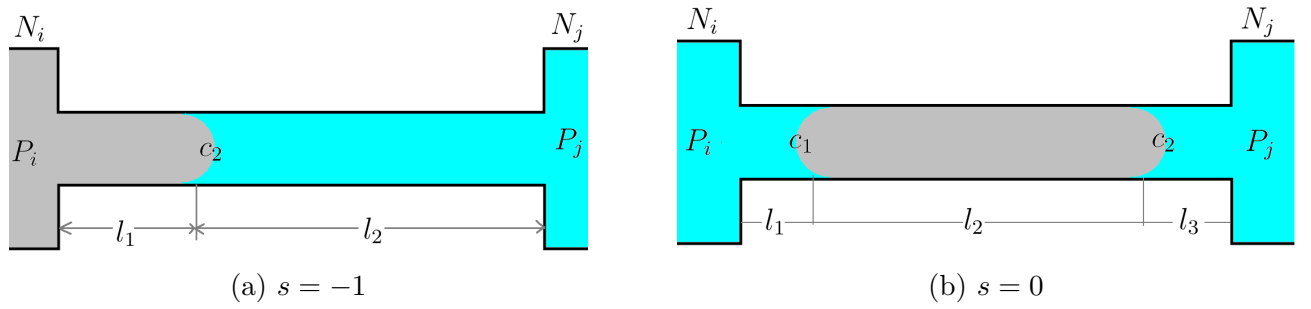

Figure 9: Capillary pressure contribution.

2.8   Flow rate and velocity

Therefore, in equation 10, we get:

$$A_{ij} = \frac{\pi R_{ij}^4}{8 M_{ij} l} \Delta P_{ij} \tag{40}$$

$$B_{ij} = \frac{\pi R_{ij}^4}{8 M_{ij} l} \frac{2 s_{ij} \sigma}{R_{ij}} \tag{41}$$

Here, note that:

$$R_{ij} = R_{ji} \tag{42}$$

$$M_{ij} = M_{ji} \tag{43}$$

$$P_{ij} = -P_{ji} \tag{44}$$

$$s_{ij} = -s_{ji} \tag{45}$$

It clear that:

$$A_{ij} = A_{ji} \tag{46}$$

$$B_{ij} = -B_{ji} \tag{47}$$

When the pressures are known in each nodes, the velocity is determined by:

$$v_{ij} = \frac{Q_{ij}}{\pi R_{ij}^2} = \frac{R_{ij}^2}{8 M_{ij} l} \left(\Delta P_{ij} + \frac{2 s_{ij} \sigma}{R_{ij}} \right) \tag{48}$$

3   Methods and examples of simulation

3.1   Algorithm for the simulation

1. **Input constants:** declare μ_1, μ_2, l, σ.

2. **Input files:** read radius and meniscus distribution.

3. **Random radius:** add very small random values to the radius distribution, so that there is an unique way of distributing fluids into the tubes.

4. **Create pressure matrix:** create a 0 filled augmented matrix M_{ij} of n rows and $n + 1$ columns, where n is the number of nodes in our system, this matrix will be solved to find the pressures in each node.

5. **Set time:** set the physical time of our simulation $t = 0$.

6. **Main loop:** until a certain saturation S is reached in a given region, or for a fixed number of frames:

    (a) **Generate linear equations:** iterate for every N_i, $1 \leq i \leq n$:

        i. **Generate connections:** the list of nodes N_j and tubes b_{ij}, which are connected to N_i.

        ii. **Iterate connections:** for each node N_j connected to N_i:

            A. R_{ij} is obtained from radius distribution. Calculate M_{ij} and s_{ij} from current meniscus configuration of b_{ij}.

            B. Using R_{ij}, M_{ij}, s_{ij}, and other constants, calculate A_{ij} and B_{ij} according to equations 40 and 41.

            C. Perform the following modifications to M_{ij}:

            $M_{ii} = M_{ii} + A_{ii}$

            $M_{ij} = M_{ij} - A_{ij}$

            $M_{i,n+1} = M_{i,n+1} - B_{ij}$

    (b) **Calculate pressures:** solve M_{ij}. Gaussian-elimination was used for the results of simulations shown in this article.

    (c) **Calculate velocity:** from the pressures calculated in each node, determine the velocity in each tube using equation 48.

    (d) **Calculate time step:** the time step for integration $\Delta t = min(\Delta t_{ij})$, here $\Delta t_{ij} = c_t min(l/v_{ij})$ for each tube b_{ij}. $c_t = 0.1$ was used for the simulations.

(e) **Calculate volume displacement**, the volume displaced in each tube is determined by, $V_{ij} = v_{ij}\Delta t$.

(f) **Store distribution:** iterate through each tube, and store how much of which fluid enters into the node towards which there is positive velocity.

(g) **Integration:** iterate through all the nodes, and for each node N_i:

    i. **List outflow tubes:** determine which tubes take away fluid from N_i.

    ii. **Distribute** the wetting and non-wetting fluids according to the algorithm described in 2.4.

    iii. **Recombine** when a tube has more than 2 menisci, according to 2.5.

(h) **Picture:** save a picture of the current configuration.

(i) **Update saturation:** calculate the new saturation S.

(j) **Update time:** $t = t + \Delta t$.

(k) **Add plot point:** add (t, S) to the plot.

7. **Video:** a video file is generated from the pictures.

3.2 Modeling simple filtration: open boundaries

In a system with closed boundaries, no fluid can enter or leave the system. For the whole system, we have:

$$\frac{\partial S}{\partial t} = 0 \tag{49}$$

In a system with open boundaries, there is at least one node, into which fluid is externally added, and at least one node through which fluid leaves.

Figure 1b is an example of a system with open boundaries. We use open boundaries to test filtration. The nodes though which any amount of fluid can enter or leave is maintained at constant pressure.

(b) Wetting fluid invading due to external pressure.
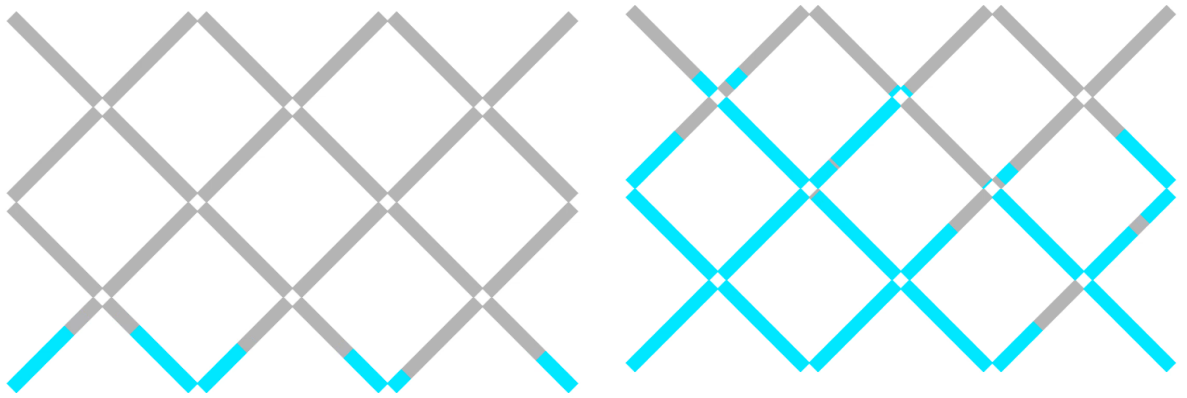
(a) Initial, wetting fluid confined to the bottom.

Figure 10: Filtration with open boundaries.

Figure 10a consists of radius different thickness. A higher pressure is fixed for all nodes in the bottom layer, while a low pressure is fixed for the top row.

3.3   Solution for closed boundaries

In an open system, the matrix is of the form 13, and an unique solution always exists. However we will now show that the set of linear equations for a system with closed boundaries has infinitely many solutions.
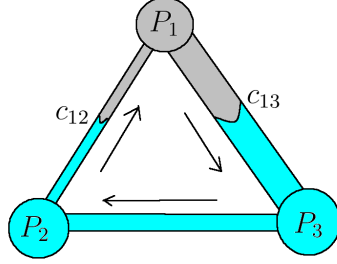

Figure 11: Infinitely many solutions for a system with 3 nodes.

The flow rates for N_1, according to equation 10:

$$Q_{12} = A_{12}(P_1 - P_2) + B_{12} \tag{50}$$

$$Q_{13} = A_{13}(P_1 - P_3) + B_{13} \tag{51}$$

Due to conservation of volume:

$$Q_{12} + Q_{13} = 0 \tag{52}$$

So, we obtain:

$$(A_{12} + A_{13})P_1 - A_{12}P_2 - A_{13}P_3 = -B_{12} - B_{13} \tag{53}$$

Applying the same for N_2 and N_3, we obtain the augmented matrix:

$$\begin{pmatrix} (A_{12} + A_{13}) & -A_{12} & -A_{13} & -B_{12} - B_{13} \\ -A_{21} & (A_{21} + A_{23}) & -A_{23} & -B_{21} - B_{23} \\ -A_{31} & -A_{32} & (A_{31} + A_{32}) & -B_{31} - B_{32} \end{pmatrix} \tag{54}$$

From equation , we have $B_{ij} = -B_{ji}$. So, the sum of all columns are zeros.

After applying $R_3 = R_3 + R_1 + R_2$ to the matrix:

$$\begin{pmatrix} (A_{12} + A_{13}) & -A_{12} & -A_{13} & -B_{12} - B_{13} \\ -A_{21} & (A_{21} + A_{23}) & -A_{23} & -B_{21} - B_{23} \\ 0 & 0 & 0 & 0 \end{pmatrix} \tag{55}$$

We obtain a zero row. This problem is solved by adding a constant a to one of the column of the matrix for every row.

$$\begin{pmatrix} (A_{12} + A_{13}) & -A_{12} & -A_{13} + a & -B_{12} - B_{13} \\ -A_{21} & (A_{21} + A_{23}) & -A_{23} + a & -B_{21} - B_{23} \\ -A_{31} & -A_{32} & (A_{31} + A_{32}) + a & -B_{31} - B_{32} \end{pmatrix} \tag{56}$$

This is the general case, when we have an arbitrary configuration of capillary pressures. In figure 11, $B_{21} = c_{12}, B_{13} = -c_{13}, B_{32} = 0$. Now, after $R_3 = R_3 + R_1 + R_2$:

$$\begin{pmatrix} (A_{12} + A_{13}) & -A_{12} & -A_{13} + a & -B_{12} - B_{13} \\ -A_{21} & (A_{21} + A_{23}) & -A_{23} + a & -B_{21} - B_{23} \\ 0 & 0 & 3a & 0 \end{pmatrix} \tag{57}$$

$$3aP_3 = 0 \tag{58}$$

The solution exists only if $P_3 = 0$. This is point of zero pressure. In our simulation, the center was chosen to be the point of zero pressure. Changing this point does not change the flow rates or the nature of flows.

3.4 Example of meniscus reaching a node: closed boundary

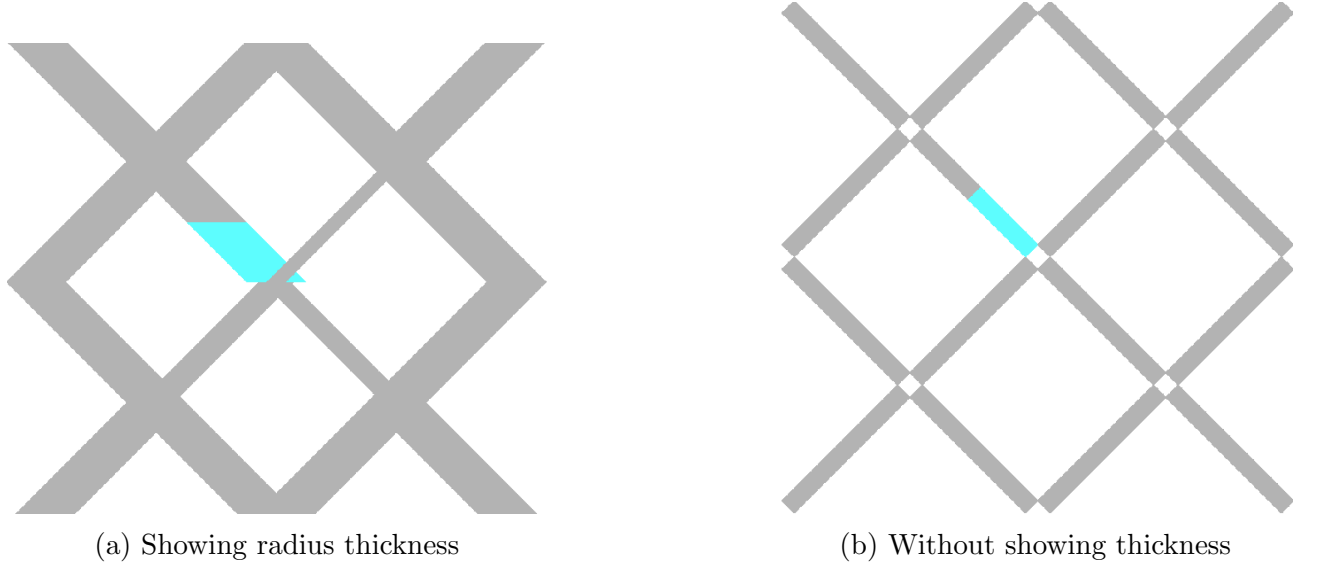(a) Showing radius thickness   (b) Without showing thickness

Figure 12: A meniscus just reached a node.

The tube where the cyan fluid is initially located is the thickest. After reaching the node, an additional 3 menisci are created very close to the node. Since the new tubes are all thinner than the initial. The capillary force from the new tubes is higher.

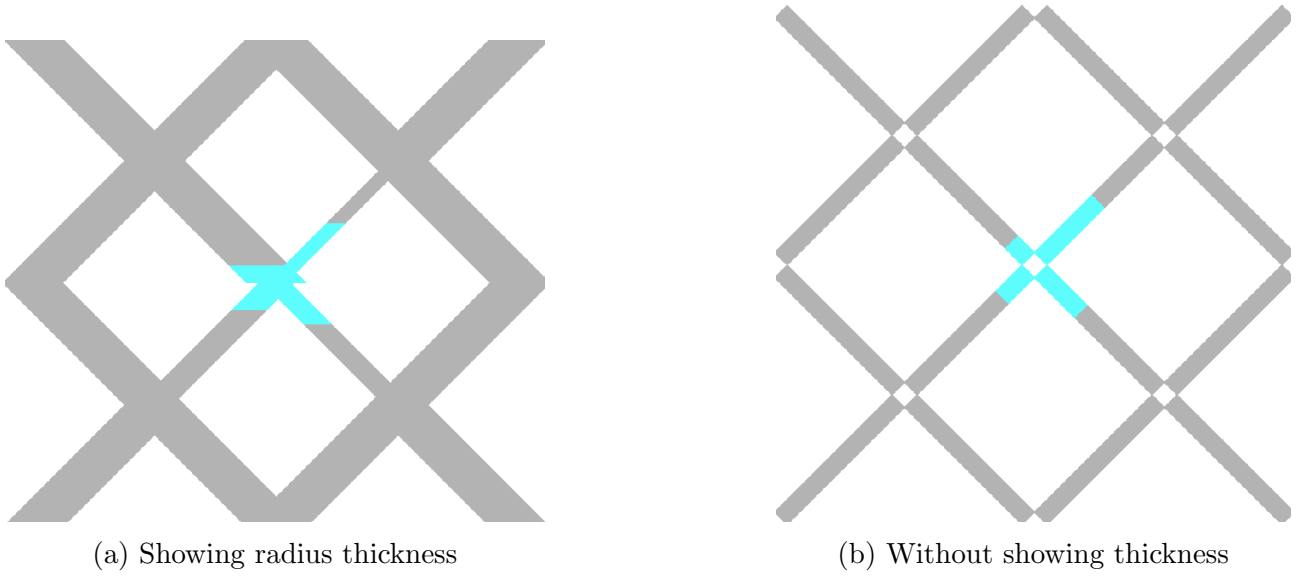(a) Showing radius thickness   (b) Without showing thickness

Figure 13: Cyan fluid being pulled by thinner tubes.

The thinnest tube pulls the cyan fluid away from the node the most, due to higher capillary pressure.

4 Experiment and results

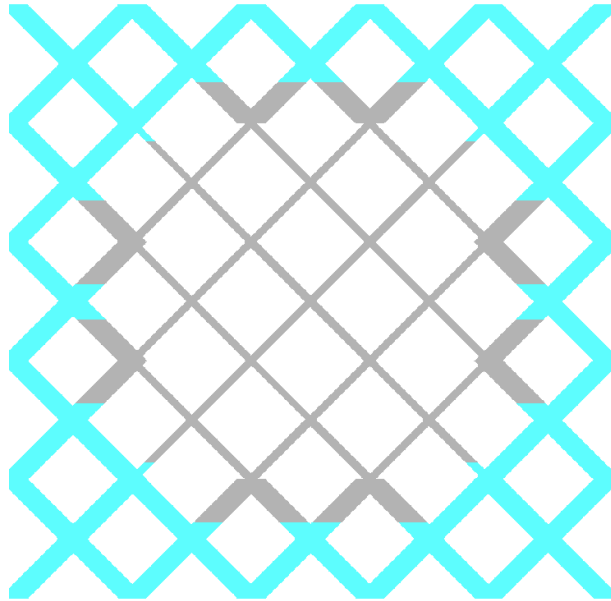## 4.1 Objective and initial conditions

Figure 14: Initial setup example, non-wetting fluid initially located in the region with thinner radii.

Our objective is to model imbibition. In figure , all of the wetting fluid is located in the outer region, which has thicker radius. The inner region is filled with non-wetting fluid. In this

simulation we wish to analyze the saturation of cyan fluid in the inner region with respect to time, $S = S(t)$. The features of the system are:

- The boundaries are closed.

- The radius in the outer region is 3 times larger, $R_{outer} = 3 * R_{inner}$.

- The size of the system is 26 x 26 tubes.

- Initially the volumes of wetting and non-wetting fluids in the whole system are equal. $V_w = V_{nw}$

4.2   Experiment (similar thickness)

The algorithm was implemented in C++ 17, compiled using gcc 9.4.0. The computation was performed using processor 11th Gen Intel Core i5-1135G7 @ 2.40GHz operating with Ubuntu 20.04 LTS. The program was not paralleled, hence only one core of the processor was used at a time. The simulation was done for 20,000 steps. Visualization of meniscus configuration and a plot point of saturation $S(t)$ was made for every 200 steps. It took about 1 minute to compile the whole program, and 5 minutes to simulate. If only the radius or initial meniscus configurations are changed, then recompiling is not required. The node located in the center of the system was chosen to have zero pressure. It was observed that changing the node which will have 0 pressure does not change the geometry of the flow.
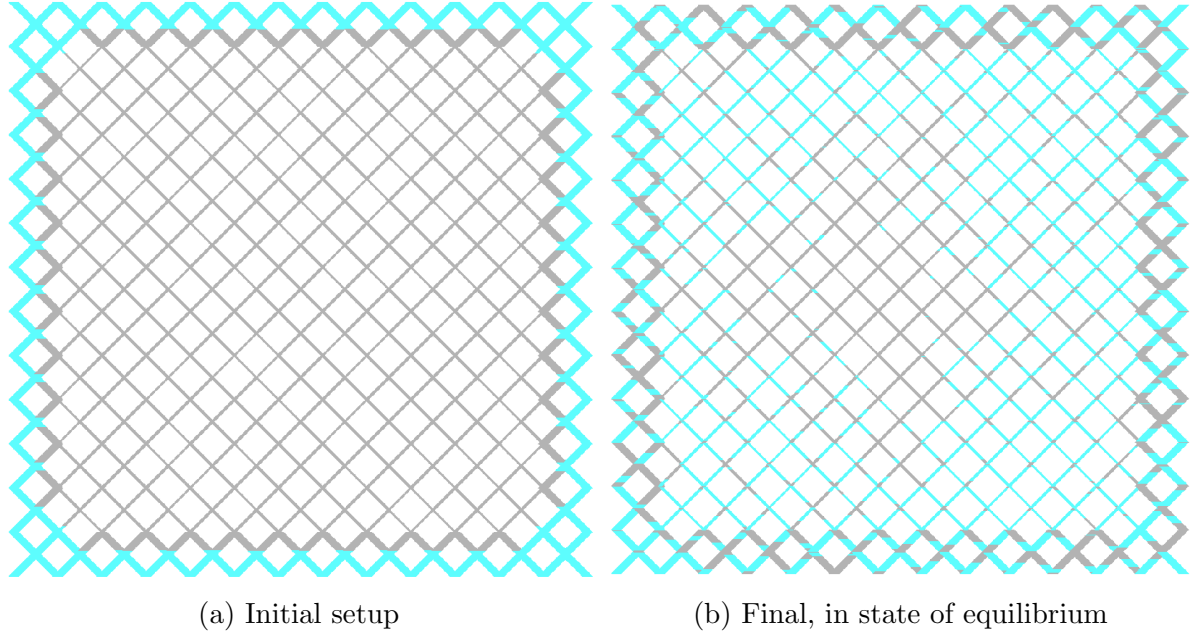

(a) Initial setup   (b) Final, in state of equilibrium

Figure 15: Plots of main experiment

The plots are not symmetric because small random values $\Delta R/R$ 10^{-3} was introduced to the system. The cyan fluid has invaded from the corners. We decided to plot for $26x26$ because a network model of this size can be easily simulated on a personal computer in a short time, and also it satisfies the conditions of gray and cyan fluids having about equal volumes, and the inner radius being 3 times thinner than the outer radius.

The the part of the program slowing down the simulation is the solution of the linear equations using Gaussian-elimination. The process of Gaussian-elimination was not optimized. Hence, if we have m variables, the time complexity for solution is m^3. If our network model is of size nxn tubes, then the number of nodes is in the order of n^2. Therefore the time to compute grows with the size of the network model in the order of n^6. If we doubled the size of the network model, it would take $2^6 = 64$ times longer to perform the same simulation, which is about 5 hours on a personal computer, still reasonable time.

For implementing the algorithm, $double$ is recommended over $float$. $float$ was earlier used to speed up the process by about 2 times, however the errors grew significantly. The saturation is supposed to remain same due to closed boundaries, but it differed by as much as 10% by the end of the simulation. The error in terms of volume of one of the fluid differing was less than 1% when $double$ was used.

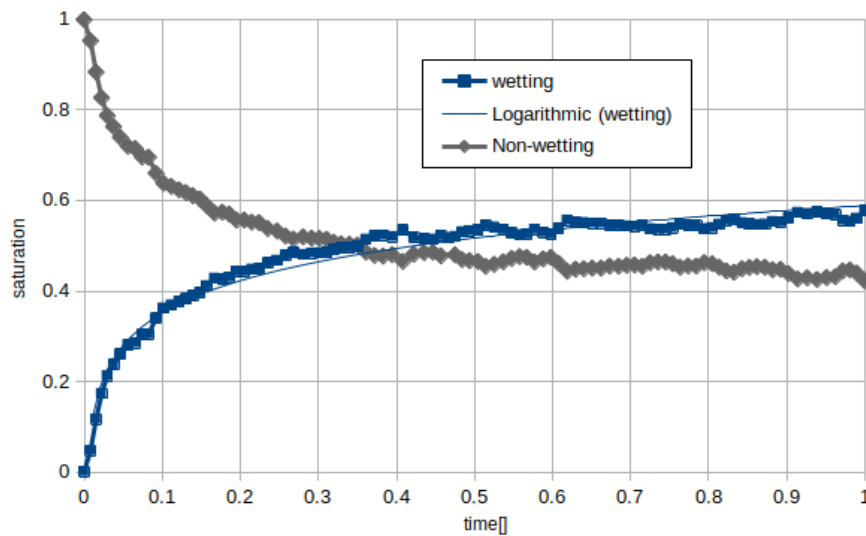## 4.3 Discussion (similar thickness)

Figure 16: Plot of saturation of cyan fluid in inner region with respect to dimensionless time.

The equilibrium saturation for wetting fluid, $S_{eq} = 0.57$ for the inner region. For different viscosity ratio μ_1/μ_2, the shape of the plot of $S(t)$ does not significantly differ. Changing constants of the experiment such as μ, σ, l simply changes the scale of the $x - axis$. Since the experiment was not calibrated to actual values, we decided to present our result in dimensionless time. It is obtained by simply diving the values on the $x - axis$ by the maximum.

In in $S(t)$ plot of cyan fluid in the inner region. Initially the rate of invasion accelerates at a high rate, then the acceleration slows down, and finally the saturation reaches an equilibrium value which shows only irregular small oscillations. These irregular oscillations is expected to disappear on using a larger network model. They occur to the blocks of wetting fluid remaining in the outer region.

The invasion of cyan fluid occurred from the corners, because in the corners each node is subjected to capillary forces more than from the middle of the edges. And the gray fluid was pushed out from the middle of the edges. The flow stops because of a large number of tubes

ending up with 2 menisci. Tubes with two meniscus have a zero net capillary pressure, and cannot initiate flows.

$S(t)$ approximately shows a logarithmic dependence. It is clear that the relaxation parameter ξ can be applied here the saturation converges to an equilibrium value.

4.4   Experiment (varying thickness)

In the previous experiment very slight difference in average capillary pressure is observed when the final saturation of wetting fluid is changed in the inner region. 10 experiments were conducted on 30 x 30 networks with varying radii in the inner region. The initial saturation of the wetting fluid was increased by increasing the proportion of wetting fluid in the inner region. Experiment 2- 10 was done for 10,000 steps. Experiment 1 for 3400 steps and experiment 2 for 1000 steps. This is because in experiment 1 - 2, at some moment complete equilibrium was achieved. There were no tubes with odd number of meniscus remaining in the system, therefore no capillary pressure to drive the flow.

The average capillary pressure at the end is calculated by taking the average of P_c according to equation 14 in the last 2000 steps of computation for experiments 2 - 10. Averaging was done to smoothing the effects of the vibrations observed in the capillary pressure. However for experiments $1 - 2$, the capillary pressure is not the average of some steps, but for the 1000th step and the 3400th step respectively.

Note that at the step when the experiment was forced to be terminated, capillary pressure cannot be defined. Since the total area in the denominator is zero. Radii of 2, 3, 4, 5 +- 0.01 was used in the inner region. Radius of 6 +- 0.01 was used in the outer region. The outer region was approximately half of the total volume.

Also, it was compulsory to add or substract 0.01 randomness to the radius distributions, because in lower initial saturation of blue fluid in the system, a flow will not start.

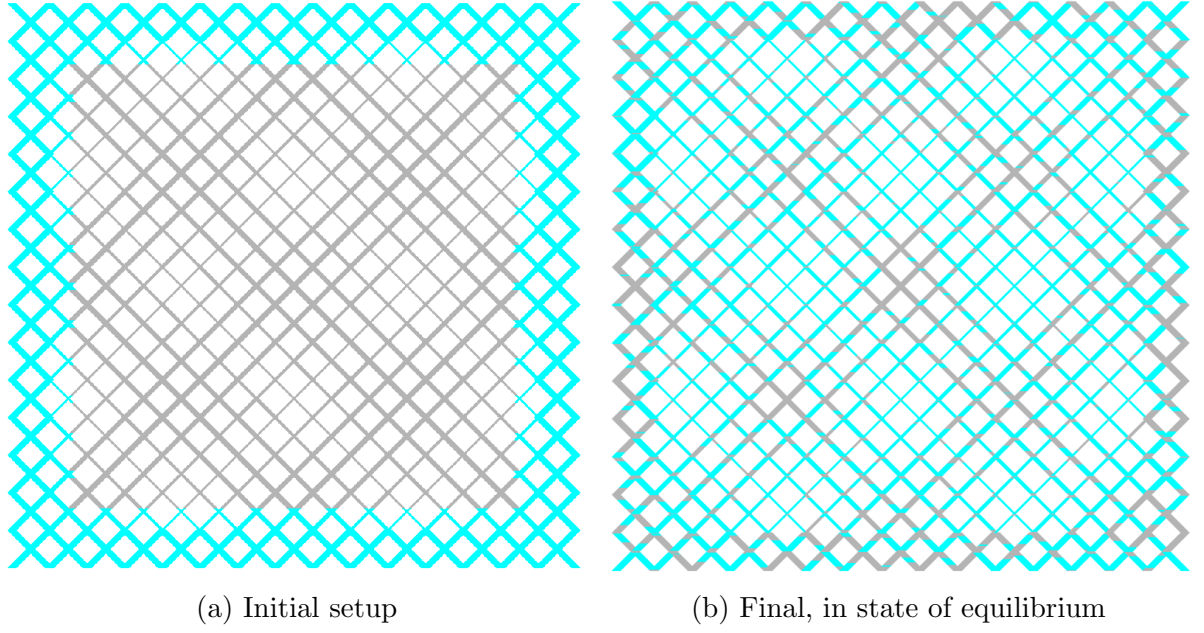(a) Initial setup   (b) Final, in state of equilibrium

Figure 17: Plots of experiment with varying thickness of tubes in the inner region. It can be seen that since it results in total lower energy of the system, it is more frequent to observe that the wetting fluid occupies the thinner tubes than the thicker tubes.

Experiment Number	Initial proportion of wetting fluid in the system	Final saturation of wetting fluid in the inner region	Average Capillary Pressure
1	0.12	0.03	0.79
2	0.20	0.12	0.68
3	0.29	0.30	0.55
4	0.43	0.46	0.54
5	0.49	0.54	0.55
6	0.53	0.58	0.54
7	0.57	0.62	0.53
8	0.60	0.65	0.54
9	0.63	0.70	0.53
10	0.66	0.73	0.53

Figure 18: Experiments conducted, with measurements on the average capillary pressure, initial amount of wetting fluid in the system, final saturation of wetting fluid in the inner region. Note that the final saturation of wetting fluid in the inner region increases with the increase of wetting fluid in the initial conditions.
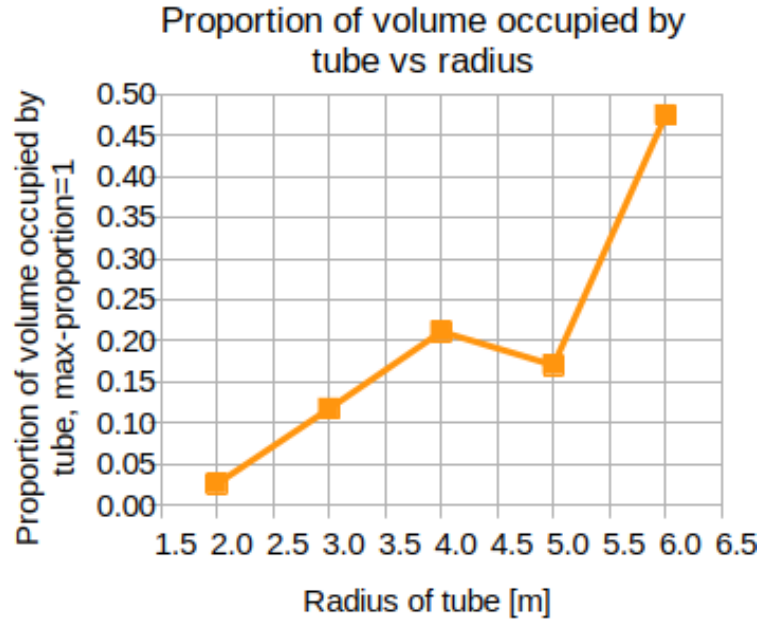
Figure 19: showing the relative volume occupied by different groups of tubes with different radii. The average capillary pressure is mainly influenced by the thinnest tubes, therefore we see that the final saturation of the wetting fluid in the inner region must be in the order of the volume of the thinnest tube in order to observe significant changes in the average capillary pressure.
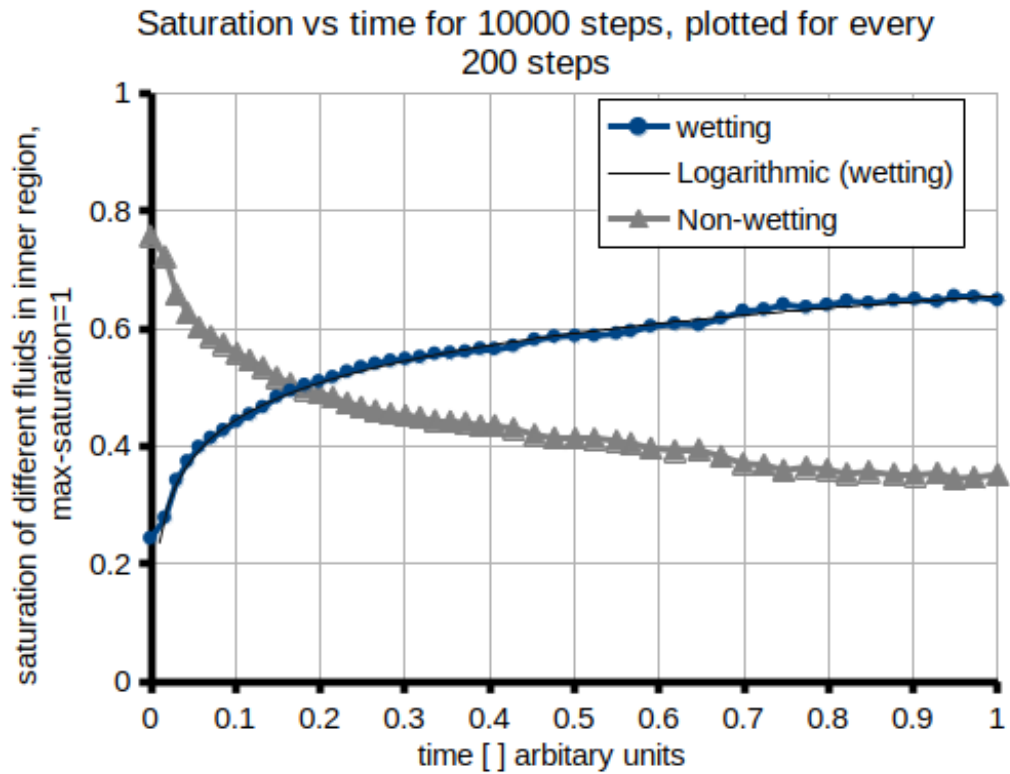

Figure 20: showing that even with varying radii in the inner region, the saturation change with respect to time remains fairly smooth.
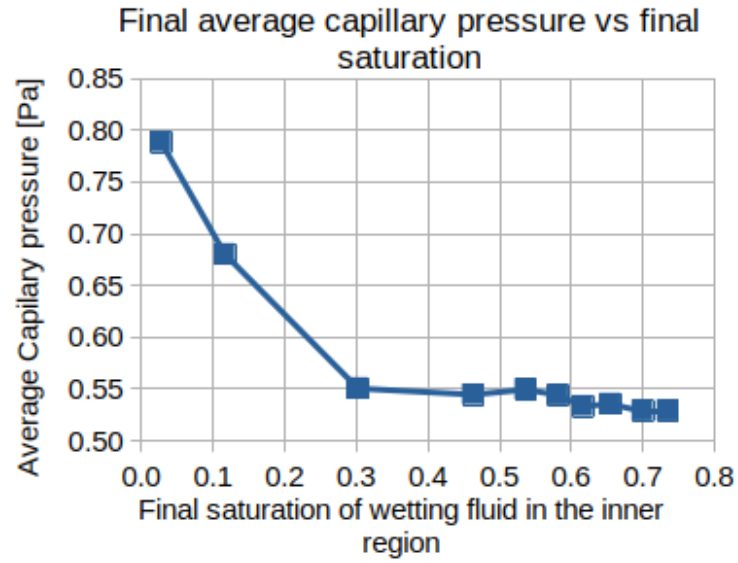
Figure 21: The average capillary pressure rapidly increases with the decrease in final saturation of wetting fluid in the inner region for very low saturations.
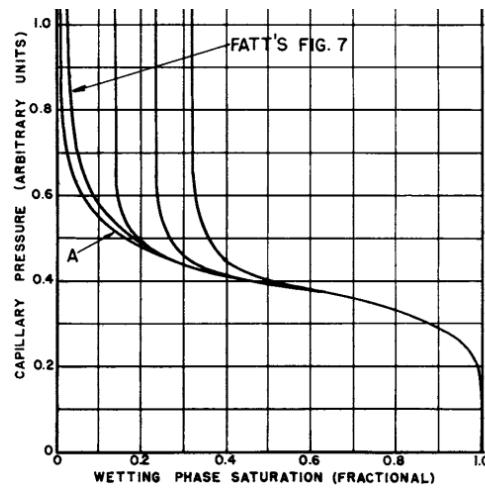

Figure 22: the dependence of capillary pressure with saturation of wetting fluid as predicted by Fratt [8]
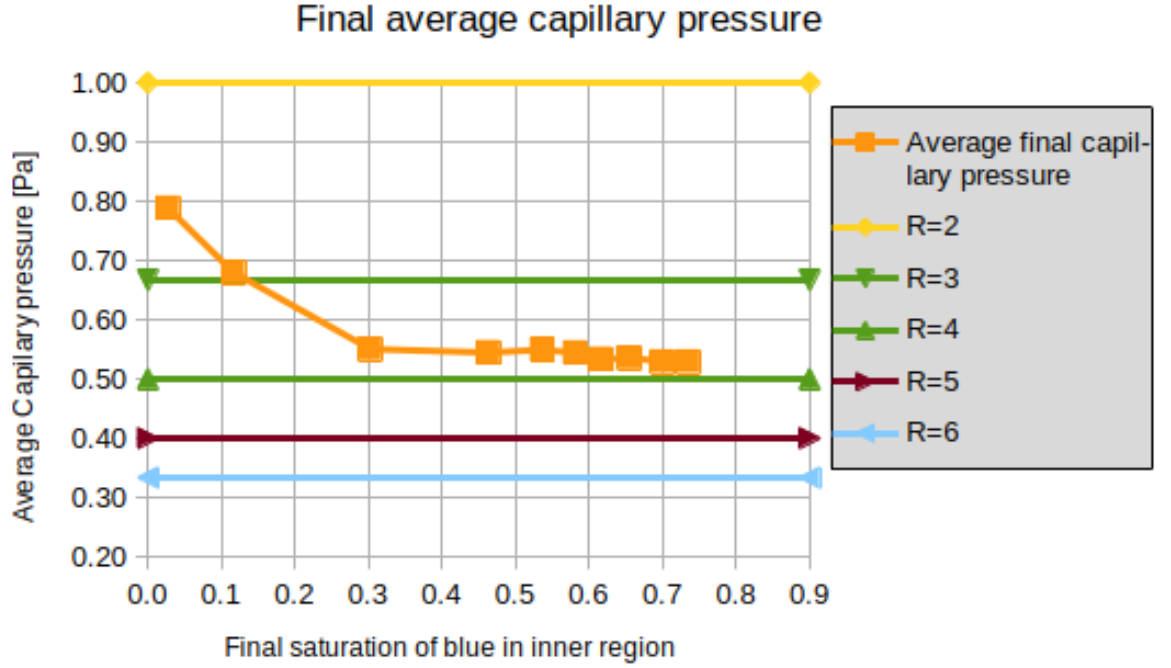
22

Figure 23: Capillary pressures in tubes of various radii denoted by horizontal straight lines, and plots of capillary pressures for various final saturations of wetting fluid in the inner region. Clearly the average caoillary pressure is situated in between the maximum and minimum horizontal bars.
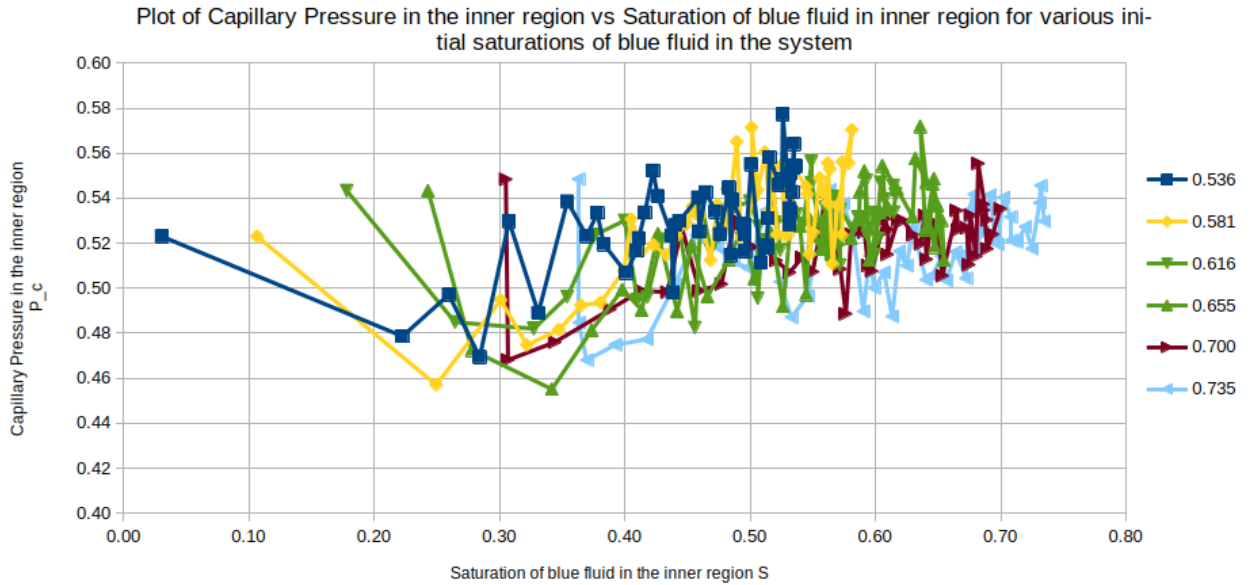

Figure 24: Capillary pressure and saturation points for every 200 steps, for high final saturation of wetting fluid in the inner region. We see that the plots tends to end similarly, however has drastically different initial capillary pressure due to the number of single menisci thinner tubes increased.

4.5 Discussion (varying thickness)

The final average capillary pressure increased with decreasing the final saturation of wetting (cyan) fluid in the inner region. However since overall less number of meniscus is created in the system is less, we face steps in the experiment where the there is no odd number of meniscus in any tube, and therefore no capillary pressure to continue flow. Therefore for lower than 0.35 initial proportions of blue fluid in the system, the experiment was required to be stopped after a certain number of steps. Since the values of Capillary pressure varied greatly between the 200 steps at which the measurement was recorded, an average of 1000 steps could not be made, therefore further investigation is required to be sure about the increase in capillary pressure.

5 Conclusions

1. The novel method of distributing different fluids in the nodes, such the wetting fluid first goes into the tube with the thinner radius is valid, since it can model imbibition, where the saturation tends to an equilibrium value.

2. The fact that the saturation $S(t)$ tends to an equilibrium value, implies that our network model can be used to simulate other relaxation phenomena, and it will help us better understand the physical meaning of the Kondaurov parameter ξ.

3. The maximum number of connections a node in our network model can have is 4. Our algorithm can be easily extended to the more connects per node. Hence the same algorithm can be used to simulate a 3 dimensional network model.

4. The fluctuations, once the saturation reaches an equilibrium value is very small. Also the error in terms of fluid lost in a closes system is extremely small. The errors were extremely small because Gaussian-elimination was used to find the pressure in each node, which is more accurate than iterative methods.

5. Our custom definition of calculating the average capillary pressure in a network model must be correct because the capillary pressure increases with decrease of saturation of wetting fluid in the inner region.

6 Acknowledgments

References

[1] Cyrus K Aidun and Jonathan R Clausen. Lattice-boltzmann method for complex flows. *Annual review of fluid mechanics*, 42:439–472, 2010.

[2] Eyvind Aker, Knut JØrgen MÅlØy, Alex Hansen, and G George Batrouni. A two-dimensional network simulator for two-phase flow in porous media. *Transport in porous media*, 32:163–186, 1998.

[3] GI Barenblatt, TW Patzek, and DB Silin. The mathematical model of nonequilibrium effects in water-oil displacement. *SPE journal*, 8(04):409–416, 2003.

[4] Grigory I Barenblatt, Iu P Zheltov, and IN Kochina. Basic concepts in the theory of seepage of homogeneous liquids in fissured rocks [strata]. *Journal of applied mathematics and mechanics*, 24(5):1286–1303, 1960.

[5] Maria C Bravo and Mariela Araujo. Analysis of the unconventional behavior of oil relative permeability during depletion tests of gas-saturated heavy oils. *International journal of multiphase flow*, 34(5):447–460, 2008.

[6] Jing-Den Chen and David Wilkinson. Pore-scale viscous fingering in porous media. *Physical review letters*, 55(18):1892, 1985.

[7] Shiyi Chen and Gary D Doolen. Lattice boltzmann method for fluid flows. *Annual review of fluid mechanics*, 30(1):329–364, 1998.

[8] I Fatt. The network model of porous media. 3. dynamic properties of networks with tube radius distribution. *Transactions of the American institute of mining and metallurgical engineers*, 207(7):164–181, 1956.

[9] Yanbin Gong. *Dynamic Pore Network Modeling of Two-Phase Flow and Solute Transport in Disordered Porous Media and Rough-Walled Fractures*. University of Wyoming, 2021.

[10] S Majid Hassanizadeh. Continuum description of thermodynamic processes in porous media: Fundamentals and applications. *Modeling Coupled Phenomena in Saturated Porous Materials*, pages 179–223, 2004.

[11] S Majid Hassanizadeh, Michael A Celia, and Helge K Dahle. Dynamic effect in the capillary pressure–saturation relationship and its impacts on unsaturated flow. *Vadose Zone Journal*, 1(1):38–57, 2002.

[12] S Majid Hassanizadeh and William G Gray. High velocity flow in porous media. *Transport in porous media*, 2:521–531, 1987.

[13] S Majid Hassanizadeh and William G Gray. Mechanics and thermodynamics of multiphase flow in porous media including interphase boundaries. *Advances in water resources*, 13(4):169–186, 1990.

[14] S Majid Hassanizadeh and William G Gray. Thermodynamic basis of capillary pressure in porous media. *Water resources research*, 29(10):3389–3405, 1993.

[15] M King Hubbert. Darcy's law and the field equations of the flow of underground fluids. *Transactions of the AIME*, 207(01):222–239, 1956.

[16] V Joekar-Niasar, S Majid Hassanizadeh, and HK Dahle. Non-equilibrium effects in capillarity and interfacial area in two-phase flow: dynamic pore-network modelling. *Journal of fluid mechanics*, 655:38–71, 2010.

[17] PR King. The fractal nature of viscous fingering in porous media. *Journal of Physics A: Mathematical and General*, 20(8):L529, 1987.

[18] VI Kondaurov. The thermodynamically consistent equations of a thermoelastic saturated porous medium. *Journal of applied mathematics and mechanics*, 71(4):562–579, 2007.

[19] VI Kondaurov. A non-equilibrium model of a porous medium saturated with immiscible fluids. *Journal of Applied Mathematics and Mechanics*, 73(1):88–102, 2009.

[20] Andrey Konyukhov, Leonid Pankratov, and Anton Voloshin. The homogenized kondaurov type non-equilibrium model of two-phase flow in multiscale non-homogeneous media. *Physica Scripta*, 94(5):054002, 2019.

[21] N Labed, L Bennamoun, and JP Fohr. Experimental study of two-phase flow in porous media with measurement of relative permeability. *Fluid Dyn. Mater. Process*, 8(4):423–436, 2012.

[22] Stephen B Pope and Stephen B Pope. *Turbulent flows*. Cambridge university press, 2000.

[23] Harris Sajjad Rabbani. *Pore-scale investigation of wettability effects on two-phase flow in porous media*. The University of Manchester (United Kingdom), 2018.

[24] Amir Raoof and S Majid Hassanizadeh. A new method for generating pore-network models of porous media. *Transport in porous media*, 81:391–407, 2010.

[25] Santanu Sinha, Andrew T Bender, Matthew Danczyk, Kayla Keepseagle, Cody A Prather, Joshua M Bray, Linn W Thrane, Joseph D Seymour, Sarah L Codd, and Alex Hansen. Effective rheology of two-phase flow in three-dimensional porous media: experiment and simulation. *Transport in porous media*, 119:77–94, 2017.

[26] Cameron Tropea, Alexander L Yarin, John F Foss, et al. *Springer handbook of experimental fluid mechanics*, volume 1. Springer, 2007.

[27] Grétar Tryggvason, Bernard Bunner, Asghar Esmaeeli, Damir Juric, N Al-Rawahi, W Tauber, J Han, S Nas, and Y-J Jan. A front-tracking method for the computations of multiphase flow. *Journal of computational physics*, 169(2):708–759, 2001.

[28] Markus Uhlmann. An immersed boundary method with direct forcing for the simulation of particulate flows. *Journal of computational physics*, 209(2):448–476, 2005.

[29] Per H Valvatne and Martin J Blunt. Predictive pore-scale modeling of two-phase flow in mixed wet media. *Water resources research*, 40(7), 2004.

[30] Edward W Washburn. The dynamics of capillary flow. *Physical review*, 17(3):273, 1921.

[31] Wikipedia. Capillary action — Wikipedia, the free encyclopedia. `http://en.wikipedia.org/w/index.php?title=Capillary%20action&oldid=1155129318`, 2023. [Online; accessed 19-June-2023].

[32] Wahyu Perdana Yudistiawan, Sang Kyu Kwak, and Santosh Ansumali. Higher order galilean invariant lattice boltzmann model. In *The 6th International Conference for Mesoscopic Methods in Engineering and Science*, page 28, 2009.